An axisymmetrical B-spline model for the non-linear free inflation of rubberlike membranes

Erwan Verron, Gilles Marckmann

▶ **To cite this version:**

Erwan Verron, Gilles Marckmann. An axisymmetrical B-spline model for the non-linear free inflation of rubberlike membranes. Computer Methods in Applied Mechanics and Engineering, 2001, 190 (46-47), pp.6271-6289. 10.1016/S0045-7825(01)00227-4 . hal-01004983

HAL Id: hal-01004983
https://hal.science/hal-01004983

Submitted on 6 Oct 2016

HAL is a multi-disciplinary open access archive for the deposit and dissemination of scientific research documents, whether they are published or not. The documents may come from teaching and research institutions in France or abroad, or from public or private research centers.

L'archive ouverte pluridisciplinaire **HAL**, est destinée au dépôt et à la diffusion de documents scientifiques de niveau recherche, publiés ou non, émanant des établissements d'enseignement et de recherche français ou étrangers, des laboratoires publics ou privés.

Distributed under a Creative Commons Public Domain Mark| 4.0 International License

An axisymmetric B-spline model for the non-linear inflation of rubberlike membranes

E. Verron [1] and G. Marckmann

Laboratoire de Mécanique et Matériaux, Division Structures, École Centrale de Nantes, BP 92101, 44321 Nantes cedex 3, France

Abstract

A new B-spline interpolation model for the free inflation of axisymmetric rubberlike membranes is presented in this paper. The membrane coordinates are interpolated by cubic B-splines and the treatment of the spline boundary conditions is highlighted. Both circular and cylindrical cases are considered. The formulation of the element is detailed and formula for the tangent operator are presented. In order to solve the non-linear system of equations, the Newton-Raphson algorithm is successfully associated with the arc-length method. Some numerical examples are presented to validate our approach and to exhibit convergence properties of the method.

Key words: B-spline model, Hyperelasticity, Axisymmetric membrane inflation, Non-linear procedure, Arc-length method

1 Introduction

The free inflation of hyperelastic rubberlike membranes has been extensively studied in the past. Two different approaches are used to solve this type of problem.

Most of the works are based on the continuum theory of Green and Adkins [10]. Analytical solutions were developed for simple cases such as the inflation of infinite cylinders [1] or spherical membranes [3]. In the most general context of clamped membranes, the problem reduces to a non-linear system of first order differential equations with two points boundary conditions. Klingbeil and Shield focused on the inflation of a circular plane membrane [15]. They used a logarithmic strain energy function to model the rubber behaviour. Later,

[1] Corresponding author: erwan.verron@ec-nantes.fr

Kydoniefs and Spencer examined the special case of the inflation of a finite cylinder clamped with a rigid annular, by using an analytical solution [16]. At the same time, general axisymmetric problems were solved using different numerical methods by Feng and coworkers [26], [32]. The authors encountered difficulties due to the unstable nature of the equilibrium path. Later Benedict *et al.* derived the governing equations of the simultaneous inflation and elongation of a cylinder [4]. Depending on the elongation ratio, they determined the limiting pressure between stable and unstable branches of the equilibrium path. Using a similar method, Wineman extended the previous results to the case of non-linear viscoelastic membranes using the K-BKZ constitutive equation [30]. More recently, Khayat *et al.* detailed the occurrence of unstable behaviours in the inflation of neo-Hookean membranes with non-uniform radius and thickness [13].

The second approach proposed in literature is based on the application of the finite element method to the problems of membrane inflation. The first paper on the subject was produced by Oden and Sato [19] and set the foundation of a Galerkin finite element approach to solve inflation problems. More recently Charrier *et al.* studied the free and confined inflation of neo-Hookean axisymmetric membranes [5]. Their developments were focused on the simulation of the blow-moulding and thermoforming processes. In the same context Khayat and Derdouri developed a hybrid finite element / finite difference algorithm to study the free and confined inflation of Mooney-Rivlin membranes [14]. A simplified approach based on the use of Biot stresses in governing equations was proposed by Jiang and Haddow in 1995. Their method was successfully applied to the case of the initially circular plane membrane [12]. Moreover, the problem of unstable solutions and secondary paths was thoroughly examined by Duffet and Reddy [9]. More recently, Shi and Moita [24] used the finite element formulation developed previously by Wriggers and Taylor [31] with an arc-length method to overcome limit points and to calculate secondary branches.

In the present paper, a spline model of axisymmetric rubberlike membrane is formulated. Attention is confined to the free inflation of both cylindrical and spherical Mooney-Rivlin membranes using a smooth interpolation in terms of cubic B-splines. In the next Section, the B-spline model is presented. The interpolation of the membrane geometry is detailed and the choice of the boundary conditions of the spline functions is examined in relation with the nature of the membrane. The governing equations of the problem are established in Section 3. After recalling the kinematics of the problem, the out-of-balance force vector is derived using the interpolation and the tangent stiffness matrix is explicitly calculated. The Section 4 is devoted to the numerical procedure used to solve the problem. The classical Newton-Raphson procedure is associated with a continuation method in order to overcome limit points. Here, the arc-length condition is considered as a bordered equation. In order to show the capability

of our model, illustrative numerical results are presented in Section 5. Finally, concluding remarks are given in the last Section.

2 The B-spline element

2.1 Definition

First, basic definitions of splines are recalled. The reader can refer to [7] for more details.

Consider an interval $[a, b] \subset \mathbb{R}$ partitioned in m subintervals by a set of $m+1$ knots $(\xi^i)_{i=0,m}$ with $\xi^0 = a$ and $\xi^m = b$. A function $f : [a, b] \to \mathbb{R}$ is a polynomial spline of degree l (l is a positive integer) if it satisfies the two following conditions:

(*i*) f is $\mathcal{C}_{l-1}$ continuous on $[a, b]$,
(*ii*) f is a polynomial function of degree l on each subinterval $[\xi^i, \xi^{i+1}[$ for $i = 0, \ldots, m-1$

It can be shown that the set of polynomial splines of degree l associated with the set of knots $(\xi^i)_{i=0,m}$ is a linear space of dimension $m+l$ [11]. This space is noted $S_l\{(\xi^i)_{i=0,m}\}$. In classical applications, linear ($l = 1$), quadratic ($l = 2$) and cubic ($l = 3$) splines are the most widely used.

"Basic Spline Curves" were first introduced by Schoenberg [22], [23]. These special spline functions were defined as a basis of $S_l\{(\xi^i)_{i=0,m}\}$. They are usually referred as *B-splines*. In the present paper we only focus on cubic B-splines defined on $[0, 1]$. Using previous notations we have $a = 0$ and $b = 1$, and the linear space of splines is $S_3\{(\xi^i)_{i=0,m}\}$ which dimension is $m + 3$. A spline f of $S_3\{(\xi^i)_{i=0,m}\}$ has a unique expansion in terms of the B-splines basis:

$$f(\xi) = \sum_{i=-1}^{m+1} v^i \, B^i(\xi) \tag{1}$$

where $(v^i)_{i=-1,m+1}$ are the parameters of the spline f and $(B^i(\xi))_{i=-1,m+1}$ are

piecewise polynomial functions defined by:

$$B^i(\xi) = \begin{cases} 0 & \xi \leq \xi^{i-2} \\ \frac{(\xi-\xi^{i-2})^3}{(\xi^{i+1}-\xi^{i-2})(\xi^{i}-\xi^{i-2})(\xi^{i-1}-\xi^{i-2})} & \xi^{i-2} \leq \xi < \xi^{i-1} \\ \frac{(\xi-\xi^{i-2})^2(\xi^{i}-\xi)}{(\xi^{i+1}-\xi^{i-2})(\xi^{i}-\xi^{i-2})(\xi^{i}-\xi^{i-1})} + \frac{(\xi^{i+1}-\xi)(\xi-\xi^{i-1})(\xi-\xi^{i-2})}{(\xi^{i+1}-\xi^{i-1})(\xi^{i}-\xi^{i-1})(\xi^{i+1}-\xi^{i-2})} & \\ \quad + \frac{(\xi-\xi^{i-1})^2(\xi^{i+2}-\xi)}{(\xi^{i+1}-\xi^{i-2})(\xi^{i}-\xi^{i-1})(\xi^{i+2}-\xi^{i-1})} & \xi^{i-1} \leq \xi < \xi^{i} \\ \frac{(\xi^{i+1}-\xi)^2(\xi-\xi^{i-2})}{(\xi^{i+1}-\xi^{i-2})(\xi^{i+1}-\xi^{i-1})(\xi^{i+1}-\xi^{i})} + \frac{(\xi^{i+2}-\xi)(\xi^{i+1}-\xi)(\xi-\xi^{i-1})}{(\xi^{i+2}-\xi^{i-1})(\xi^{i+1}-\xi^{i-1})(\xi^{i+1}-\xi^{i})} & \\ \quad + \frac{(\xi^{i+2}-\xi)^2(\xi-\xi^{i})}{(\xi^{i+2}-\xi^{i-1})(\xi^{i+2}-\xi^{i})(\xi^{i+1}-\xi^{i})} & \xi^{i} \leq \xi < \xi^{i+1} \\ \frac{(\xi^{i+2}-\xi)^3}{(\xi^{i+2}-\xi^{i-1})(\xi^{i+2}-\xi^{i})(\xi^{i+2}-\xi^{i+1})} & \xi^{i+1} \leq \xi < \xi^{i+2} \\ 0 & \xi^{i+2} \leq \xi \end{cases} \quad (2)$$

with the following conventions:

- $\xi^i = \xi^0$ for $i \leq 0$,
- $\xi^i = \xi^m$ for $i \geq m$,
- with these two conventions some denominators are equal to 0 and we adopt the equality: $0/0 = 0$

Figure 1 presents the B-spline function corresponding to a knot i.

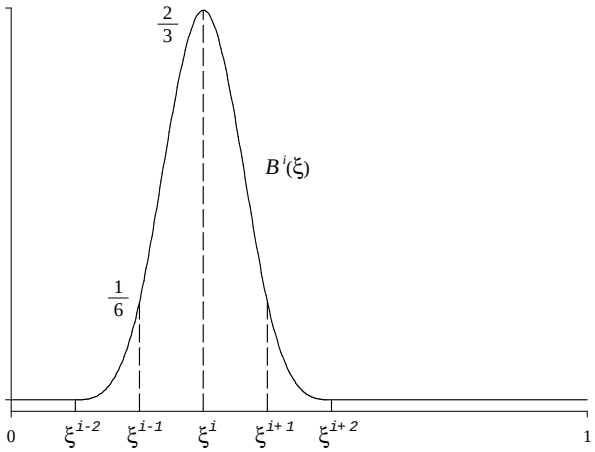

Fig. 1. The B-spline $B^i(\xi)$

2.2 Interpolation of a two-dimensional curve

2.2.1 Membrane interpolation

It will be shown later that the geometry of the undeformed axisymmetric membrane is reduced to a two-dimensional continuous curve $\mathcal{L}$. Each material point P of the curve is positioned by $(R(s), Z(s))$ where s is the adimensional arc-length coordinate which varies from 0 to 1 along the curve, and $R(s)$ and $Z(s)$ are respectively the undeformed radial and axial coordinates. The curve is divided in n parts. Boundaries of these parts are $n+1$ points $(N^j)_{j=0,n}$ and are called nodes, similarly to the classical finite element method vocabulary. Coordinates of the node N^j are denoted (R^j, Z^j) and its arc-length coordinate is s^j.

Consider now an arbitrary set of m knots on $\mathcal{L}$: $\Omega_{\mathcal{L}} = (\xi^i)_{i=0,m}$. Previous coordinates $R(s)$ and $Z(s)$ can be interpolated by two cubic splines, i.e. two elements of $S_3\{\Omega_{\mathcal{L}}\}$:

$$R(s) = \sum_{i=-1}^{m+1} \alpha^i B^i(s) \tag{3}$$

$$Z(s) = \sum_{i=-1}^{m+1} \beta^i B^i(s) \tag{4}$$

where $(\alpha^i)_{i=-1,m+1}$ and $(\beta^i)_{i=-1,m+1}$ are the parameters of the two splines. For each spline, the $m+3$ parameters have to be determined in an unique manner: $m+3$ independent equations are needed. Taking into account boundary conditions which provide two equations, only $m+1$ interpolation equations have to be considered. Therefore the choice $m = n$ becomes obvious. In other words the number of knots is set equal to the number of interpolated nodes. In the present work, knots coordinates are chosen such that they correspond to the arc-length coordinates of the nodes:

$$\xi^i = s^i \qquad \text{for } i = 0, \ldots, n \tag{5}$$

The arc-length coordinate and the number of knots (and nodes) will be respectively denoted s and n throughout the rest of paper.

2.2.2 Boundary conditions

As mentioned above, boundary conditions provide two additional linear equations. Two different types of boundary conditions have to be examined depending whether a boundary node lies on the symmetry axis or not. Only the case of the first node N^0 is detailed. Similar developments can be carried out for the last node N^n.

First we consider the case where the first node is not in the symmetry axis. In that case, natural end conditions for both interpolations are considered [11]:

$$R''(0) = 0 \tag{6}$$
$$Z''(0) = 0 \tag{7}$$

In these equations the superscript prime denotes the differentiation with respect to s. Using Eqs (6) and (7) as the two additional equations, interpolating splines (3) and (4) can be written as terminated series of only $n+1$ modified B-splines functions:

$$R(s) = \sum_{i=0}^{n} \alpha^i \, B_r^i(s) \tag{8}$$
$$Z(s) = \sum_{i=0}^{n} \beta^i \, B_z^i(s) \tag{9}$$

where the two modified B-splines sequences $B_r^i(s)_{i=0,n}$ and $B_z^i(s)_{i=0,n}$ are given by:

$$B_r^i(s) = \begin{cases} \dfrac{-2s^0 + s^1 + s^2}{s^2 - s^0} B^{-1} + B^0(s) & \text{for } i = 0 \\ \dfrac{s^0 - s^1}{s^2 - s^0} B^{-1} + B^1(s) & \text{for } i = 1 \\ B^i(s) & \text{for } i = 2, \ldots, n-2 \\ \text{depends on the boundary condition at } N^n & \text{for } i = n-1, n \end{cases} \tag{10}$$

for the radial coordinate interpolation and by exactly the same definitions for the interpolation of the axial coordinate, said $B_z^i(s)_{i=0,n}$.

Consider now the case where the first node lies on the symmetry axis. The two splines have not the same boundary condition in N^0. As the node must remain on the axis we have: $R(0) = 0$. Then the boundary condition for the radial coordinate is a natural end condition similarly to the previous case: $R''(0) = 0$. It implies that the modified B-splines $B_r^i(s)_{i=0,n}$ are given by Eq. (10). For the axial coordinate $Z(s)$, an Hermite end boundary condition should be considered:

$$Z'(0) = 0 \tag{11}$$

Using this condition the modified B-splines relative to the axial coordinate are given by:

$$B_z^i(s) = \begin{cases} B^{-1} + B^0(s) & \text{for } i = 0 \\ B^i(s) & \text{for } i = 1, \ldots, n-2 \\ \text{depends on the boundary condition at } N^n & \text{for } i = n-1, n \end{cases} \tag{12}$$

In that case the two sequences of the new interpolation functions are different.

2.2.3 Displacement interpolation and differentiation properties

Similarly to the classical Finite Element Method, our element is considered isoparametrical: displacements are interpolated using the same basis functions as those used in the geometrical splines (3) and (4). Radial and axial displacements are respectively denoted $u_r(s)$ and $u_z(s)$, and are interpolated by two new splines:

$$u_r(s) = \sum_{i=0}^{n} \gamma^i \, B_r^i(s) \tag{13}$$

$$u_z(s) = \sum_{i=0}^{n} \delta^i \, B_z^i(s) \tag{14}$$

in which $(\gamma^i)_{i=0,n}$ and $(\delta^i)_{i=0,n}$ are the parameters of the two splines.

In order to determine the previous spline parameters, two square matrices $\mathbf{A_r}$ and $\mathbf{A_z}$ of dimension $n+1$ are introduced. Generic terms A_r^{ij} of $\mathbf{A_r}$ and A_z^{ij} of $\mathbf{A_z}$ are respectively given by:

$$A_r^{ij} = B_r^j(s^i) \tag{15}$$

$$A_z^{ij} = B_z^j(s^i) \tag{16}$$

and the parameters $(\alpha^i)_{i=0,n}$, $(\beta^i)_{i=0,n}$, $(\gamma^i)_{i=0,n}$ and $(\delta^i)_{i=0,n}$ can be obtained by using the previous interpolation formula (3), (4), (13) and (14) at the nodes and solving the four linear systems of equations:

$$\sum_{j=0}^{n} A_r^{ij} \alpha^j = R^i \qquad \text{for } i = 0, n \tag{17}$$

$$\sum_{j=0}^{n} A_z^{ij} \beta^j = Z^i \qquad \text{for } i = 0, n \tag{18}$$

$$\sum_{j=0}^{n} A_r^{ij} \gamma^j = u_r^i \qquad \text{for } i = 0, n \tag{19}$$

$$\sum_{j=0}^{n} A_z^{ij} \delta^j = u_z^i \qquad \text{for } i = 0, n \tag{20}$$

in which (u_r^i, u_z^i) stands for the displacements of the node N^i.

Now deformed radial and axial coordinates of the membrane material points $(r(s), z(s))$ can be easily calculated by:

$$r(s) = R(s) + u_r(s) = \sum_{i=0}^{n} B_r^i(s) \, (\alpha^i + \gamma^i) \tag{21}$$

$$z(s) = Z(s) + u_z(s) = \sum_{i=0}^{n} B_z^i(s) \, (\beta^i + \delta^i) \tag{22}$$

Moreover, using previous interpolations (21) and (22), and linear relations (19) and (20), useful derivative formulas are established:

$$\frac{\partial r}{\partial u_r^i}(s) = \sum_{j=0}^{n} B_r^j(s)\, A_r^{\star ji} \qquad \frac{\partial r}{\partial u_z^i}(s) = 0 \tag{23}$$

$$\frac{\partial z}{\partial u_r^i}(s) = 0 \qquad \frac{\partial z}{\partial u_z^i}(s) = \sum_{j=0}^{n} B_z^j(s)\, A_z^{\star ji} \tag{24}$$

$$\frac{\partial r'}{\partial u_r^i}(s) = \sum_{j=0}^{n} B_r^{j'}(s)\, A_r^{\star ji} \qquad \frac{\partial r'}{\partial u_z^i}(s) = 0 \tag{25}$$

$$\frac{\partial z'}{\partial u_r^i}(s) = 0 \qquad \frac{\partial z'}{\partial u_z^i}(s) = \sum_{j=0}^{n} B_z^{j'}(s)\, A_z^{\star ji} \tag{26}$$

in which matrices $\mathbf{A_r^\star}$ and $\mathbf{A_z^\star}$ are the respective inverses of $\mathbf{A_r}$ and $\mathbf{A_z}$. Using these equations, new useful functions $D_r^i(s)_{i=0,n}$ and $D_z^i(s)_{i=0,n}$, and their derivatives with respect to s, $D_r^{i'}(s)_{i=0,n}$ and $D_z^{i'}(s)_{i=0,n}$, are defined by:

$$D_r^i(s) = \sum_{j=0}^{n} B_r^j(s)\, A_r^{\star ji} \tag{27}$$

$$D_z^i(s) = \sum_{j=0}^{n} B_z^j(s)\, A_z^{\star ji} \tag{28}$$

and:

$$D_r^{i'}(s) = \sum_{j=0}^{n} B_r^{j'}(s)\, A_r^{\star ji} \tag{29}$$

$$D_z^{i'}(s) = \sum_{j=0}^{n} B_z^{j'}(s)\, A_z^{\star ji} \tag{30}$$

These functions will be used in the next part to simplify the discretization of equilibrium equations. Note that they have to be computed only once just after having defined the number of knots and the type of boundary conditions.

3 Governing equations

3.1 Problem kinematics and constitutive equation

Consider the free inflation of a rubberlike membrane. The material is assumed homogeneous, isotropic, incompressible and elastic, and the membrane is a cylinder of non-uniform radius and uniform thickness in the undeformed configuration. The thickness is considered much less than any radius of curvature and the membrane geometry is described by the position of its mid-surface.

The undeformed and deformed mid-surface configurations are respectively denoted $\mathcal{B}_0$ and $\mathcal{B}$. A particle P of $\mathcal{B}_0$ is located using the cylindrical polar coordinates system (R, Θ, Z). After deformation, the same particle is located at (r, θ, z) on the deformed configuration $\mathcal{B}$. Due to the axial symmetry the particle motion is given by:

$$r = R + u_r \tag{31}$$
$$\theta = \Theta \tag{32}$$
$$z = Z + u_z \tag{33}$$

where u_r and u_z are respectively the radial and axial displacements of P as defined in the previous part. Consequently, the undeformed membrane geometry is reduced to an one-dimensional continuum curve of length L. Undeformed and deformed coordinates, respectively (R, Z) and (r, z), and thickness, respectively H and h, are functions of one independent variable [32]. Here the reduced arc-length coordinate s is chosen. Note that s varies from 0 to 1 as the real arc-length varies from 0 to L.

Moreover, principal stretch directions are known and the three corresponding principal stretch ratios in the meridian, circumferential and radial directions are respectively defined as:

$$\lambda_1 = \sqrt{\frac{r'^2 + z'^2}{R'^2 + Z'^2}} \quad , \quad \lambda_2 = \frac{r}{R} \quad , \quad \lambda_3 = \frac{h}{H} \tag{34}$$

and the corresponding components of the Green-Lagrange strain tensor $\mathbf{E}$ are:

$$E_i = \frac{\lambda_i^2 - 1}{2} \qquad \text{for } i = 1, 3 \tag{35}$$

Due to incompressibility the third stretch ratio λ_3 is eliminated using the relation $\lambda_1 \lambda_2 \lambda_3 = 1$ and the thickness of the deformed body is simply obtained by using the following equation:

$$h = \frac{1}{\lambda_1 \lambda_2} H \tag{36}$$

Finally we introduce the outward normal to the surface $\mathbf{n}$, which will be relevant for the definition of loads:

$$\mathbf{n} = \left\{ \begin{array}{c} \dfrac{z'}{\sqrt{r'^2 + z'^2}} \\ -\dfrac{r'}{\sqrt{r'^2 + z'^2}} \end{array} \right\} \tag{37}$$

These definitions are summarized in Fig. 2.

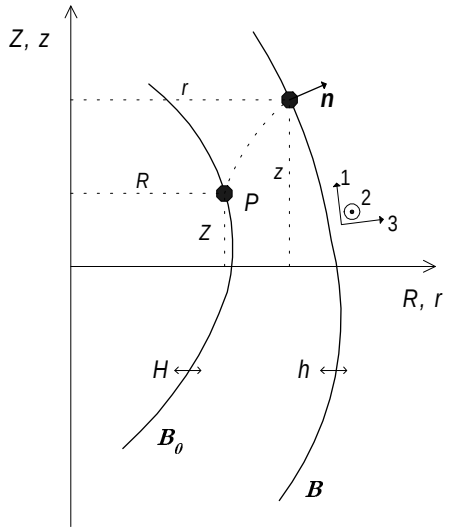

Fig. 2. Inflation of an axisymmetric membrane: geometry.

In this paper we only examine the case of the Mooney-Rivlin constitutive equation [18]. In the special case of incompressible materials, the corresponding strain energy density function can be written in terms of λ_1 and λ_2:

$$W = C\left[\left(\lambda_1^2 + \lambda_2^2 + \lambda_1^{-2}\lambda_2^{-2} - 3\right) + \alpha\left(\lambda_1^{-2} + \lambda_2^{-2} + \lambda_1^2\lambda_2^2 - 3\right)\right] \tag{38}$$

where C and α are the two parameters of the material. In the case $\alpha = 0$ the model reduces to the neo-Hookean constitutive equation [27]. Considering that the membrane is in a plane stress state, principal stresses of the second Piola-Kirchhoff stress tensor are expressed as:

$$S_1 = 2C\left(1 - \frac{1}{\lambda_1^4\lambda_2^2}\right)\left(1 + \alpha\lambda_2^2\right) \tag{39}$$

$$S_2 = 2C\left(1 - \frac{1}{\lambda_1^2\lambda_2^4}\right)\left(1 + \alpha\lambda_1^2\right) \tag{40}$$

$$S_3 = 0 \tag{41}$$

respectively in the meridian, circumferential and axial directions.

3.2 Principle of Virtual Work

Ignoring inertia and body forces, the Principle of Virtual Work can be written in the following form:

$$g(\mathbf{u}, \delta\mathbf{u}, p) = \int_{\mathcal{B}_0} \delta W \, dV - \int_{\partial\mathcal{B}} \delta\mathbf{u}\, p\, \mathbf{n}\, dS = 0 \qquad \forall\, \delta\mathbf{u} \tag{42}$$

in which p is the internal blowing pressure, $\delta\mathbf{u}$ stands for a virtual displacement vector and $\partial\mathcal{B}$ represents the deformed membrane surface. The first integral

term is the virtual work of internal forces and the second integral term is the virtual work of external loading forces. Note that the work of external forces is defined in the current deformed configuration because the blowing pressure force is a follower force. Using the axial symmetry, geometrical definitions (34) and (37), and stress-strain relations (39), (40) and (41), the virtual work difference $g(\mathbf{u}, \delta\mathbf{u}, p)$ simplifies:

$$g(\mathbf{u}, \delta\mathbf{u}, p) = \int_0^1 2\,\pi\,R\,L\,H\;\left(S_1\,\lambda_1\,\delta\lambda_1 + S_2\,\lambda_2\,\delta\lambda_2\right)\,ds \\ - \int_0^1 2\,\pi\,p\,r\;\left(\delta u_r\,z' - \delta u_z\,r'\right)\,ds \quad (43)$$

Now the membrane is divided in n segments delimited by $n+1$ nodes $(N^i)_{i=0,n}$. Thus, using the previous developments, the Principle of Virtual Work can be expressed as:

$$g(\mathbf{u}, \delta\mathbf{u}, p) = \delta\mathbf{U}^T\,\mathbf{G}(\mathbf{U}, p) = 0 \qquad \forall\;\delta\mathbf{U} \quad (44)$$

In this equation $\mathbf{U}$ is the nodal displacements vector:

$$\mathbf{U} = \left\{ \begin{array}{c} \vdots \\ u_r^i \\ \\ u_z^i \\ \vdots \end{array} \right\} \quad (45)$$

and $\mathbf{G}(\mathbf{U}, p)$ is the out-of-balance force which must be equal to zero to ensure equilibrium. Moreover $\mathbf{G}(\mathbf{U}, p)$ can be written under the following form:

$$\mathbf{G}(\mathbf{U}, p) = \mathbf{F}_{\text{int}}(\mathbf{U}) - \mathbf{F}_{\text{ext}}(\mathbf{U}, p) \quad (46)$$

where $\mathbf{F}_{\text{int}}(\mathbf{U})$ and $\mathbf{F}_{\text{ext}}(\mathbf{U})$ are the internal and external forces vectors respectively.

With the previous differentiation rules (23)-(26) and functional definitions (27)-(30), the internal forces vector is:

$$\mathbf{F}_{\text{int}}(\mathbf{U}) = \int_0^1 2\,\pi\,R\,L\,H\,\mathbf{B}_{\text{nl}}\,\mathbf{S}\,ds \quad (47)$$

where the non-linear matrix $\mathbf{B}_{\text{nl}}$ is a matrix of dimension $2(n+1) \times 2$ and

relies nodal displacements to strains:

$$\mathbf{B}_{\rm nl} = \begin{bmatrix} \vdots & \vdots \\ \dfrac{r'}{dL^2} D_r^{i'}(\xi) & \dfrac{r}{R^2} D_r^i(\xi) \\ \dfrac{z'}{dL^2} D_z^{i'}(\xi) & 0 \\ \vdots & \vdots \end{bmatrix}_{i=0,n} \tag{48}$$

in which dL is defined as:

$$dL = \sqrt{R'^2 + Z'^2} \tag{49}$$

The stress vector $\mathbf{S}$ in Eq. (47) is simply:

$$\mathbf{S} = \begin{Bmatrix} S_1 \\ S_2 \end{Bmatrix} \tag{50}$$

where S_1 and S_2 are defined in Eqs (39) and (40).

Similarly the external forces vector is a vector of dimension $2(n+1)$ given by:

$$\mathbf{F}_{\rm ext}(\mathbf{U}, p) = \int_0^1 2\,\pi\, p\, \boldsymbol{\phi}\, ds \tag{51}$$

with:

$$\boldsymbol{\phi} = \begin{Bmatrix} \vdots \\ r\, z'\, D_r^i(\xi) \\ -r\, r'\, D_z^i(\xi) \\ \vdots \end{Bmatrix}_{i=0,n} \tag{52}$$

It is obvious that the system (46) is highly non-linear both geometrically and by the constitutive equation. Therefore, the classical tangent stiffness matrix has to be defined in order to solve the problem. This matrix denoted $\mathbf{K}$ is the derivative of the out-of-balance force vector $\mathbf{G}(\mathbf{U}, p)$ with respect to the nodal displacements vector $\mathbf{U}$. Using the same notations that Shi and Moita [24] used for the classical finite element method, we introduce two stiffness matrices $\mathbf{K}_{\rm int}$ and $\mathbf{K}_{\rm ext}$ defined by:

$$\mathbf{K} = \mathbf{K}_{\rm int} - \mathbf{K}_{\rm ext} = \frac{\partial \mathbf{F}_{\rm int}}{\partial \mathbf{U}} - \frac{\partial \mathbf{F}_{\rm ext}}{\partial \mathbf{U}} \tag{53}$$

In this equation the internal stiffness matrix $\mathbf{K}_{\rm int}$ is the sum of two terms:

$$\mathbf{K}_{\rm int} = \mathbf{K}_{\rm int}^{\rm I} + \mathbf{K}_{\rm int}^{\rm II} \tag{54}$$

which are given by:

$$\mathbf{K}_{\text{int}}^{\text{I}} = \int_0^1 2\,\pi\,R\,L\,H\,\left(S_1\,\frac{\partial \mathbf{B}_{\text{nl}}^{\text{col }\mathbf{1}}}{\partial \mathbf{U}} + S_2\,\frac{\partial \mathbf{B}_{\text{nl}}^{\text{col }\mathbf{2}}}{\partial \mathbf{U}}\right) ds \tag{55}$$

in which $\mathbf{B}_{\text{nl}}^{\text{col }\mathbf{1}}$ and $\mathbf{B}_{\text{nl}}^{\text{col }\mathbf{2}}$ stand for the first and second columns of $\mathbf{B}_{\text{nl}}$ respectively, and:

$$\mathbf{K}_{\text{int}}^{\text{II}} = \int_0^1 2\,\pi\,R\,L\,H\,\mathbf{B}_{\text{nl}}\frac{\partial \mathbf{S}}{\partial \mathbf{U}} ds \tag{56}$$

Similarly, the external stiffness matrix is:

$$\mathbf{K}_{\text{ext}} = \int_0^1 2\,\pi\,p\,\frac{\partial \boldsymbol{\phi}}{\partial \mathbf{U}}\,ds \tag{57}$$

The ready-to-program formulas for these two stiffness matrices are detailed in the appendix. In this work vectors and matrices integration is done by using the Simpson's method. More particularly all the examples presented in this paper were computed with 200 integration points on the membrane.

4 Non-linear numerical procedure

As mentioned above, the problem is highly non-linear. Thus an incremental-iterative approach is needed to determine equilibrium points. Moreover it is well-known that pressure-displacement curves corresponding to rubberlike membranes inflation problems exhibit limit points and 'snap-throughs' [3], [28]. This behaviour is due to the follower force produced by the inflating pressure: this force depends on the current deformed membrane surface. Consequently a continuation method has to be adopted to determine the equilibrium path [25]. Here a combination of the classical Newton-Raphson iterative method and the arc-length method is developed. The arc-length method consists of completing the system of equilibrium equations with an additional relation between the load (here the pressure) and the displacement increments. This method was first introduced by Riks [20] and various modifications were proposed [6].

Consider a particular equilibrium point on the equilibrium path. This point is defined by the displacement vector $\mathbf{U_e}$ and the inflating pressure p_e which satisfy the equilibrium equation. The goal of the numerical procedure is to find one new equilibrium point on the path. This new point is defined by displacement and pressure increments denoted $\Delta\mathbf{U}$ and Δp respectively, and it satisfies simultaneously the two following equations:

$$\begin{cases} \mathbf{G}(\mathbf{U_e} + \Delta\mathbf{U}, p_e + \Delta p) = 0 \\ \\ A(\Delta\mathbf{U}, \Delta p) = 0 \end{cases} \tag{58}$$

The first equation is the classical equilibrium equation and the second one is the arc-length equation in which the function A is given by:

$$A(\Delta\mathbf{U}, \Delta p) = \left(\|\Delta\mathbf{U}\|^2 + \psi^2 \|\Delta\mathbf{F}_{\text{ext}}\|^2\right) - da^2 \tag{59}$$

where $\Delta\mathbf{F}_{\text{ext}}$ is the increment of the external forces vector (51) corresponding to the pressure and the displacement field, ψ is a scale factor between displacement and force components and da is the arc-length which is the control parameter. In this study the factor ψ is set to zero and the method reduces to the classical displacement control method [2].

The Newton-Raphson iterative method as applied to the previous system (58) is now examined. Consider the algorithm at a given iteration, the system to be solved is:

$$\begin{cases} \mathbf{G}^{\underline{\text{n}}} = \mathbf{G}^{\underline{\text{o}}} + \dfrac{\partial \mathbf{G}}{\partial \Delta \mathbf{U}}\, \mathbf{dU} + \dfrac{\partial \mathbf{G}}{\partial \Delta p} dp = 0 \\ \\ A^{\underline{\text{n}}} = A^{\underline{\text{o}}} + \dfrac{\partial A}{\partial \Delta \mathbf{U}}\, \mathbf{dU} + \dfrac{\partial A}{\partial \Delta p}\, dp = 0 \end{cases} \tag{60}$$

where superscripts $\cdot^{\underline{\text{n}}}$ and $\cdot^{\underline{\text{o}}}$ mean respectively 'new' (for the present iteration) and 'old' (for the previous iteration), and where $\mathbf{dU}$ and dp are the respective changes in displacement and pressure. Now, next increments to be considered are given by:

$$\begin{cases} \Delta\mathbf{U}^{\underline{\text{n}}} = \Delta\mathbf{U}^{\underline{\text{o}}} + \mathbf{dU} \\ \\ \Delta p^{\underline{\text{n}}} = \Delta p^{\underline{\text{o}}} + dp \end{cases} \tag{61}$$

Using the previous definition of the tangent stiffness matrix (53) and recalling that $\psi = 0$, the system (60) becomes:

$$\begin{cases} \mathbf{G}^{\underline{\text{n}}} = \mathbf{G}^{\underline{\text{o}}} + \mathbf{K}\, \mathbf{dU} - dp\, \mathbf{f}_{\text{ext}} = 0 \\ \\ A^{\underline{\text{n}}} = A^{\underline{\text{o}}} + 2\, \Delta\mathbf{U}^{\underline{\text{o}}} \cdot \mathbf{dU} = 0 \end{cases} \tag{62}$$

where $\mathbf{f}_{\text{ext}}$ is the reduced external forces vector that only depends on the displacement field:

$$\mathbf{f}_{\text{ext}}(\mathbf{U}) = \frac{1}{p}\, \mathbf{F}_{\text{ext}}(\mathbf{U}, p) = \int_0^1 2\, \pi\, \boldsymbol{\phi}\, ds \tag{63}$$

In order to solve the problem (62), we consider the second equation of the system as a bordered equation [21]. The tangent stiffness matrix is extended and the system of equations is written as:

$$\left[\begin{array}{c|c} \mathbf{K} & -\mathbf{f}_{\text{ext}} \\ \hline 2\Delta\mathbf{U}^{\underline{\text{o}}\text{T}} & 0 \end{array}\right] \left\{\begin{array}{c} \mathbf{dU} \\ \hline dp \end{array}\right\} = - \left\{\begin{array}{c} \mathbf{G}^{\underline{\text{o}}} \\ \hline A^{\underline{\text{o}}} \end{array}\right\} \tag{64}$$

where the superscript $\cdot^{\mathrm{T}}$ stands for the transposition. It is to note that the tangent stiffness matrix $\mathbf{K}$ is non-symmetric due to the boundary conditions. Thus the previous approach can be used without changing the nature of the resolution algorithm.

In order to initiate this resolution scheme, the forward-Euler tangential predictor solution is adopted. The two predicted increments $\Delta\mathbf{U}^{\mathrm{pred}}$ and Δp^{pred} are supposed to satisfy the equilibrium equation (first equation of (62)) with $\mathbf{G}^{\underline{o}} = \mathbf{0}$:

$$\Delta\mathbf{U}^{\mathrm{pred}} = \Delta p^{\mathrm{pred}}\, \mathbf{dU}^{\mathrm{tan}} \tag{65}$$

where the tangent displacement vector $\mathbf{dU}^{\mathrm{tan}}$ is given by:

$$\mathbf{dU}^{\mathrm{tan}} = \mathbf{K}^{-1}\, \mathbf{f}_{\mathrm{ext}} \tag{66}$$

Moreover, using the arc-length equation (second equation of system (62)), the norm of the displacement predictor is considered to be equal to da:

$$\|\Delta\mathbf{U}^{\mathrm{pred}}\|^2 = da^2 \tag{67}$$

Consequently the pressure predictor to applied is given by:

$$\Delta p^{\mathrm{pred}} = \varepsilon \frac{da}{\|\mathbf{dU}^{\mathrm{tan}}\|} \qquad \text{with } \varepsilon = \pm 1 \tag{68}$$

Due to the presence of the sign factor ε, two values of the predicted pressure are possible. In order to overcome limit points this sign must be evaluated. To determine the value of ε, we consider the scalar product between the displacement increment $\Delta\mathbf{U_e}$ (increment between the two last equilibrium points) and the tangent displacement vector, and we adopt its sign:

$$\varepsilon = \mathrm{sign}\left[\Delta\mathbf{U_e} \cdot \mathbf{dU}^{\mathrm{tan}}\right] \tag{69}$$

5 Numerical results

In this part three examples are studied: the two first ones are compared with analytical solutions and the last one is used to examine the influence of the number of nodes on convergence.

5.1 Infinite cylinder

The first example is the inflation of a cylindrical membrane with infinitely long boundary conditions.

Consider a cylinder with uniform radius R_0 in the undeformed configuration. The length and the uniform thickness of the membrane are respectively L and H. The material is modeled by the Mooney-Rivlin constitutive equation and the material parameters are C and α as defined previously. The problem geometry and the boundary conditions are shown in Fig. 3(a). In that case

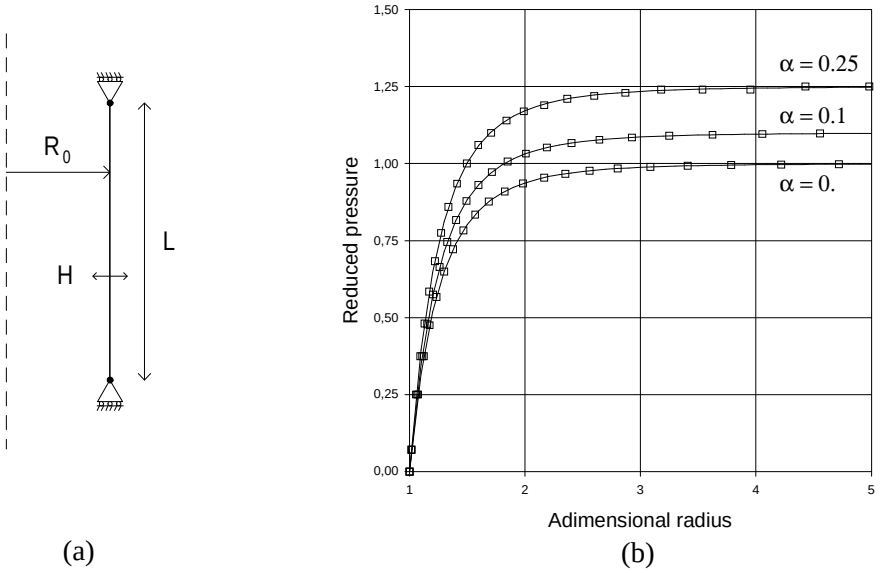

Fig. 3. Inflation of an infinite cylinder. (a) Model description. (b) Reduced pressure versus adimensional radius for different values of α: (–) analytical results, (□) numerical results.

both first and last nodes are not on the symmetry axis and their axial positions are fixed. Thus natural end boundary conditions are considered for the two extremities and for both R- and Z-interpolations.

The response under the inflating pressure P is a uniform expansion of the radius without axial expansion ($\lambda_1 = 1$). The corresponding equilibrium equation in the circumferential direction is simply [1]:

$$\sigma_2 = \frac{Pr}{h} \tag{70}$$

where σ_2 is the Cauchy stress in the circumferential direction and, r and h are the uniform deformed radius and thickness respectively. Using the relation between the Cauchy stress and the second Piola-Kirchhoff stress, i.e. $\sigma_2 = \lambda_2^2 S_2$, and the stress-strain relation (40), this equilibrium equation becomes:

$$P = \frac{2CH}{R_0}\left(1 - \frac{1}{\lambda^4}\right)(1 + \alpha) \tag{71}$$

in which λ is the adimensional radius:

$$\lambda = \lambda_2 = \frac{r}{R_0} \tag{72}$$

Introducing the reduced pressure p:

$$p = \frac{PR_0}{2CH} \tag{73}$$

Eq. (71) simplifies:

$$p = (1+\alpha)\left(1 - \frac{1}{\lambda^4}\right) \tag{74}$$

This equation provides analytical results.

Numerical results are obtained with 21 nodes on the membrane and with the following numerical data:

$$R_0 = 1. \qquad L = 10. \qquad H = 0.01 \qquad C = 1. \tag{75}$$

Three values of α are examined: $\alpha = 0.$, $\alpha = 0.1$ and $\alpha = 0.25$.

The comparison between analytical and numerical results is presented in Fig. 3(b). The inflating pressure tends to the constant value $1+\alpha$ as the cylinder inflates. The curves show that numerical computations are in very good agreement with analytical results.

5.2 Spherical membrane

In this second example the inflation of a spherical membrane is examined.

Consider a Mooney-Rivlin spherical membrane which radius and thickness in the undeformed configuration are respectively R_0 and H. Both boundary nodes lie on the symmetry axis. In these nodes a natural end boundary condition is considered for the R-interpolation and a Hermite end boundary condition is imposed for the Z-interpolation (see Section 2). The model geometry and the boundary conditions are presented in Fig. 4(a).

It is assumed that the membrane remains spherical during inflation. Therefore, due to the spherical symmetry, the problem can be reduced to an one-dimensional equilibrium equation and the pressure-adimensional radius relation is [3]:

$$P = \frac{4CH}{R_0}\left(\frac{1}{\lambda} - \frac{1}{\lambda^7}\right)\left(1 + \alpha\lambda^2\right) \tag{76}$$

where λ is the ratio between the deformed and the undeformed radii, and P is the inflating pressure. Similarly to the previous example the reduced pressure is defined by:

$$p = \frac{PR_0}{4CH} \tag{77}$$

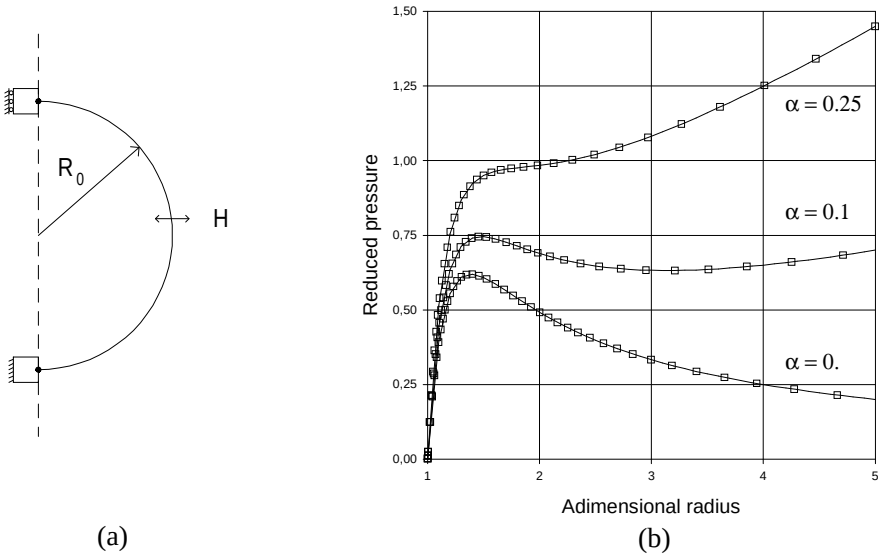

Fig. 4. Inflation of a spherical membrane. (a) Model description. (b) Reduced pressure versus adimensional radius for different values of α: (–) analytical results, (□) numerical results.

and the equilibrium equation (76) becomes:

$$p = \left(\frac{1}{\lambda} - \frac{1}{\lambda^7}\right)\left(1 + \alpha\lambda^2\right) \tag{78}$$

For the numerical simulation the membrane is meshed with 41 nodes and the following numerical values are adopted:

$$R_0 = 1. \qquad H = 0.01 \qquad C = 1. \tag{79}$$

As in the previous case three values of α are studied.

Eq. (78) was extensively examined in the past. It is well-known that the membrane exhibits three different behaviours depending on the value of the material parameter α [28]. For $\alpha = 0.$, there is one limit point and the pressure can not withstand pressures greater than the maximum pressure. In the case $\alpha = 0.1$, the curve presents two limit points and three different branches: two stable and one unstable. For $\alpha = 0.25$, the pressure always increases as the radius of the balloon increases. As shown in Fig. 4(b) numerical solutions closely fit to the analytical results in the three different cases. This demonstrates the ability of the arc-length method to follow the primary path of equilibrium and to overcome limit points.

5.3 Fully clamped cylinder

The third and last example examined in this paper is the inflation of a fully clamped cylinder. No simple analytic solution can be proposed and this problem is known to be highly unstable and difficult to solve [13].

5.3.1 Solution of the problem

Here we consider a cylindrical membrane which radius R_0 and thickness H are uniform along the membrane in the undeformed configuration. The length of the cylinder is denoted L. The material is assumed to be of Mooney-Rivlin type (the parameters are C and α). The membrane is fully clamped: axial and radial coordinates of both extreme nodes are fixed and the B-splines interpolations have natural end boundary conditions. The cylinder is inflated by a uniform pressure P. In order to simplify the discussion some adimensional variables are considered. The adimensional pressure is defined by:

$$p = \frac{PR_0}{2CH} \tag{80}$$

and the adimensional radial and axial coordinates are defined as R/R_0 and Z/R_0 respectively.

For the numerical calculations only a semi-cylinder is studied due to the symmetry with respect to the $Z = 0$ axis. A mesh of 101 nodes on the semi-cylinder is used. It will be shown later that such a mesh is sufficient to ensure convergence.

First, the evolution of the pressure versus the maximum radius is studied. Fig. 5 presents these results for three values of α. As shown in this figure the fully clamped cylinder exhibits the same behaviour as in the spherical case. Depending on the value of α the equilibrium path has one stable and one unstable branches ($\alpha = 0.$), two stable and one unstable branches ($\alpha = 0.1$) or only one stable branch ($\alpha = 0.25$).

Moreover the deformed profiles of the membrane are examined. Fig. 6 presents the deformed profiles under different inflating pressure for the three values of α. For $\alpha = 0.1$ and $\alpha = 0.25$, the membrane inflates regularly on both stable and unstable branches. The membrane with $\alpha = 0.25$ is the stiffest one: the pressure needed to inflate it until a given deformation level is ever greater that the corresponding pressures needed for the two other values of α. In the special case $\alpha = 0.$, i.e. for a neo-Hookean material, the cylinder exhibits a bulge on the unstable branch (when the pressure decreases as the maximum radius of the membrane profile increases). This observation was previously made by some authors [17], [29].

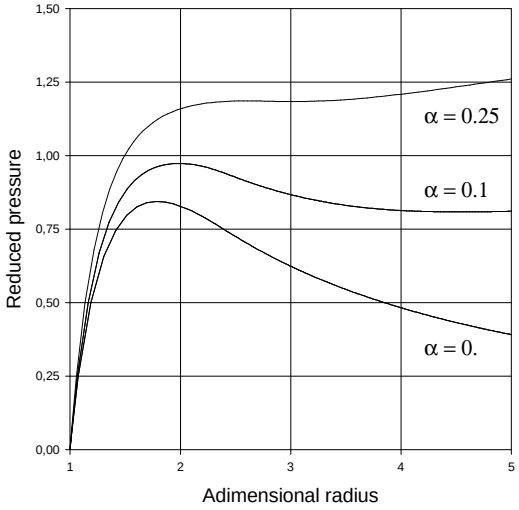

Fig. 5. Reduced pressure vs maximum radius for three values of α.

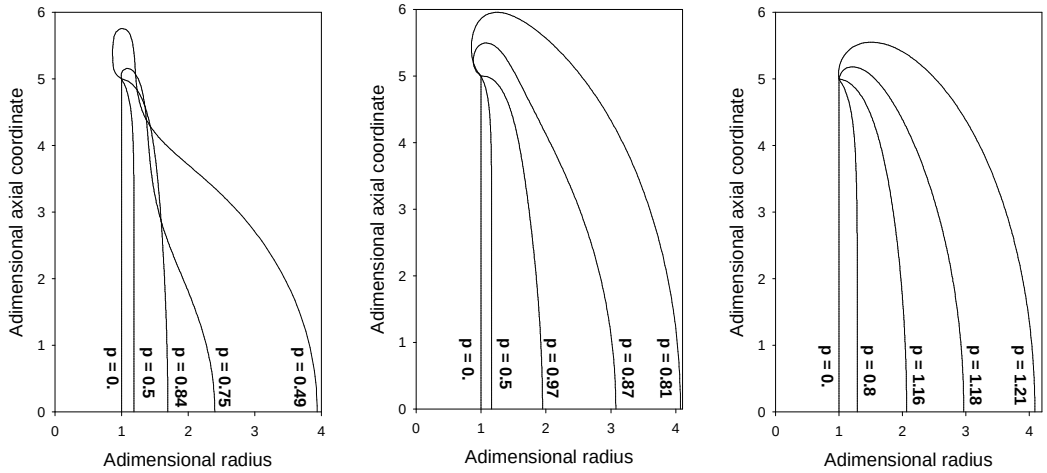

Fig. 6. Evolution of the cylinder profile during inflation: (a) $\alpha = 0.$, (b) $\alpha = 0.1$ and (c) $\alpha = 0.25$.

5.3.2 Convergence analysis

The next verification of the present approach is whether the loading curve and the membrane profiles converge to a unique solution as meshes are refined. To check this convergence property, let us examine the evolution of the solution as the number of nodes changes. The previous calculation with 101 nodes is considered as the reference solution. Six new simulations are performed for different numbers of nodes equally distributed on the undeformed membrane: 5, 11, 21, 31, 41 and 51 nodes. In order to compare the corresponding solutions with the reference solution, two convergence ratios are defined. The first one is evaluated on the loading curve (the pressure vs maximum radius curve) and is denoted R_l. It is defined as the maximum difference between the loading

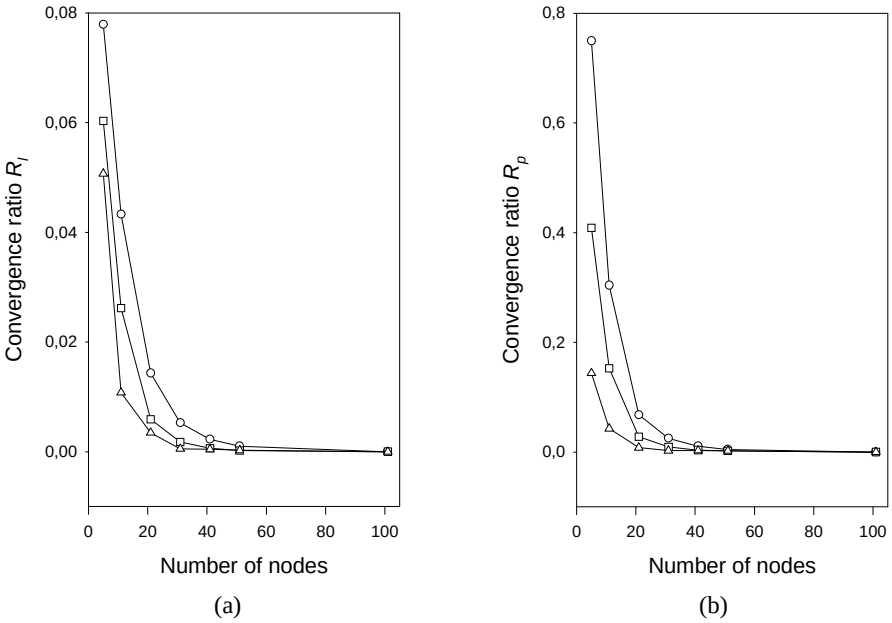

Fig. 7. Convergence properties. (a) Loading ratio R_l, (b) profiles ratio R_p: ($\circ$) $\alpha = 0.$, ($\square$) $\alpha = 0.1$ and ($\triangle$) $\alpha = 0.25$.

curves of a mesh and of the reference solution. The second ratio is used to evaluate the discrepancy of solutions for the profiles of the inflated membrane. First, distances between two profiles which have the same maximum radius are computed for all loading pressures. Then the ratio, denoted R_p, is defined as the maximum of these distances on the inflation history. Evolution of both ratios are presented in Figs 7(a) and 7(b) respectively for R_l and R_p. The two graphs are very similar. For the three values of the material parameter, we can affirm that the convergence is satisfactory around 40 nodes for the two criteria. Nevertheless the convergence speed differs depending on α. Greater is the value of α, faster is the convergence on both ratios. For cases in which some parts of the behaviour are unstable ($\alpha = 0.$ and $\alpha = 0.1$), more nodes are needed to ensure convergence than in the stable case ($\alpha = 0.25$).

6 Concluding remarks

In this paper, the use of a spline interpolation to simulate the free inflation of rubber membrane is examined. The model is build in a similar manner than the classical finite element models usually used in such cases. The geometrical coordinates of the membrane particles are interpolated by cubic B-splines. Using the same interpolation rules for the displacement field, the governing equations are discretized and the non-linear system of equations is solved by using an incremental-iterative method. Numerical results for both cylindrical and spherical membranes validate successfully our approach.

The present study will be used in further works. First, the development of contact procedures is in progress to simulate plastic forming processes. Some appropriate detection algorithms will be developed in order to take into account the smoothness of the B-spline interpolation. Secondly, our model will be joined with a fitting procedure in order to determine the constitutive equations of rubberlike materials. For this, numerical results will be compared with data obtained from bubble inflation experiments [8].

Appendix

The first term of the internal stiffness matrix (55) is rewritten as:

$$\mathbf{K}_{\text{int}}^{\text{I}} = \int_0^1 2\,\pi\,R\,L\,H\,\mathbf{k}_{\text{int}}^{\text{I}}\,ds \tag{81}$$

with:

$$\mathbf{k}_{\text{int}}^{\text{I}} = \begin{bmatrix} & \vdots & \vdots & \\ \cdots & \dfrac{S_1}{dL^2} D_r^{i'} D_r^{j'} + \dfrac{S_2}{R^2} D_r^i D_r^j & 0 & \cdots \\ \cdots & 0 & \dfrac{S_1}{dL^2} D_z^{i'} D_z^{j'} & \cdots \\ & \vdots & \vdots & \end{bmatrix} \tag{82}$$

Similarly, the second term (56) is given by:

$$\mathbf{K}_{\text{int}}^{\text{II}} = \int_0^1 2\,\pi\,R\,L\,H\,\mathbf{k}_{\text{int}}^{\text{II}}\,ds \tag{83}$$

with:

$$\mathbf{k}_{\text{int}}^{\text{II}} = \begin{bmatrix} & \vdots & \vdots & \\ \cdots & S_{11}\dfrac{r'^2}{dL^4\lambda_1} D_r^{i'} D_r^{j'} + S_{12}\dfrac{r'}{RdL^2} D_r^{i'} D_r^j & S_{11}\dfrac{r'z'}{dL^4\lambda_1} D_r^{i'} D_z^{j'} + S_{21}\dfrac{rz'}{R^2dL^2\lambda_1} D_r^i D_z^{j'} & \cdots \\ & + S_{21}\dfrac{rr'}{R^2dL^2\lambda_1} D_r^i D_r^{j'} + S_{22}\dfrac{r}{R^3} D_r^i D_r^j & & \\ \cdots & S_{11}\dfrac{r'z'}{dL^4\lambda_1} D_z^{i'} D_r^{j'} + S_{12}\dfrac{z'}{RdL^2} D_z^{i'} D_r^j & S_{11}\dfrac{z'^2}{dL^4\lambda_1} D_z^{i'} D_z^{j'} & \cdots \\ & \vdots & \vdots & \end{bmatrix} \tag{84}$$

For the external stiffness matrix (57), the same method is used:

$$\mathbf{K}_{\text{ext}} = \int_0^1 2\,\pi\,p\,\mathbf{k}_{\text{ext}}\,ds \tag{85}$$

in which:

$$\mathbf{k}_{\text{ext}} = \begin{bmatrix} & \vdots & \vdots & \\ \cdots & z' D_r^i D_r^j & r D_r^i D_z^{j'} & \cdots \\ & & & \\ \cdots & -D_z^i \left(r' D_r^j + r D_r^{j'} \right) & 0 & \cdots \\ & \vdots & \vdots & \end{bmatrix} \tag{86}$$

References

[1] H. Alexander, The tensile instability of initially spherical balloons, Int. J. Engng Sci. 9 (1971) 151–162.

[2] J. L. Batoz, G. Dhatt, Incremental displacement algorithms for nonlinear problems, Int. J. Num. Meth. Engng 14 (1979) 1262–1267.

[3] M. F. Beatty, Topics in finite elasticity: hyperelasticity of rubber, elastomers, and biological tissues - with examples, Appl. Mech. Rev. 40 (12) (1987) 1699–1734.

[4] R. Benedict, A. Wineman, W. H. Yang, The determination of limiting pressure in simultaneous elongation and inflation of nonlinear elastic tubes, Int. J. Solids Structures 15 (1979) 241-249.

[5] J. M. Charrier, S. Shrivastava, R. Wu, Free and constrained inflation of elastic membranes in relation to thermoforming - Axisymmetric problems, J. Strain Analysis 22 (2) (1987) 115–125.

[6] M. A. Crisfield, Non-linear finite element analysis of solids and structures. Volume 1: Essentials, John Wiley and Sons Ltd, Chichester, England, 1994, Ch. 9.

[7] C. De Boor, A practical guide to splines, Springer, New-York, 1978.

[8] A. Derdouri, R. Connolly, R. E. Khayat, E. Verron, B. Peseux, Material constants identification for thermoforming simulation, in: Conference Proceedings at ANTEC'98, I (Atlanta, 26-30 april 1998) 672–675.

[9] G. A. Duffet, B. D. Reddy, The solution of multi-parameter systems of equations with application to problems in nonlinear elasticity, Comp. Meth. Appl. Mech. Engng 59 (1986) 179–213.

[10] A. E. Green, J. E. Adkins, Large elastic deformations, The Clarendon Press, Oxford, 1960.

[11] G. Hammerlin, K. H. Hoffmann, Numerical mathematics, Undergraduate texts in mathematics, Springer Verlag, New-York, 1991, Ch. 6.

[12] L. Jiang, J. B. Haddow, A finite element formulation for finite static axisymmetric deformation of hyperelastic membranes, Comput. Struct. 57 (3) (1995) 401–405.

[13] R. E. Khayat, A. Derdouri, A. Garcia-Réjon, Inflation of an elastic cylindrical membrane: non-linear deformation and instability, Int. J. Solids Structures 29 (1) (1992) 69–87.

[14] R. E. Khayat, A. Derdouri, Inflation of hyperelastic cylindrical membranes as applied to blow moulding. Part I. axisymmetric case, Int. J. Numer. Meth. Engng 37 (1994) 3773-3791.

[15] W. W. Klingbeil, R. T. Shield, Some numerical investigations on empirical strain energy functions in the large axi-symmetric extensions of rubber membranes, Z. Angew. Math. Phys. 15 (1964) 608–629.

[16] A. D. Kydoniefs, J. M. Spencer, Finite axisymmetric deformations of an initially cylindrical membrane, Q. J. Mech. Appl. Math. 22 (1969) 87-95.

[17] S. Kyriakides, Y. Chang, The initiation and propagation of a localized instability in an inflated elastic tube, Int. J. Solids Struct. 27 (1991) 1085–1111.

[18] M. Mooney, A theory of large elastic deformation, J. Appl. Phys. 11 (1940) 582–592.

[19] J. T. Oden, T. Sato, Finite strains and displacements of elastic membranes by the finite element method, Int. J. Solids Struct. 3 (1967) 471–488.

[20] E. Riks, The application of Newton's method to the problem of elastic stability, J. Appl. Mech. 39 (1972) 1060–1066.

[21] E. Riks, C. C. Rankin, An incremental approach to the solution of snapping and buckling problems, Int. J. Solids Struct. 15 (1979) 529–551.

[22] I. J. Schoenberg, Contributions to the problem of equidistant data by analytic functions. Part A, Quat. Appl. Math. 4 (1) (1946) 45–97.

[23] I. J. Schoenberg, Contributions to the problem of equidistant data by analytic functions. Part B, Quat. Appl. Math. 4 (2) (1946) 112–141.

[24] J. Shi, G. F. Moita, The post-critical analysis of axisymmetric hyper-elastic membranes by the finite element method, Comput. Methods Appl. Mech. Engng 135 (1996) 265–281.

[25] T. Sokól, M. Witkowski, Some experiences in the equilibrium path determination, Comput. Assist. Mech. Engng Sci. 4 (1997) 189–208.

[26] J. T. Tielking, W. W. Feng, The application of minimum potential energy principle to axisymmetric nonlinear membrane problems, J. Appl. Mech. ASME 42 (1974) 491–497.

[27] L. R. G. Treloar, The mechanics of rubber elasticity, Proc. R. Soc. Lond. A351 (1976) 301–330.

[28] E. Verron, R. E. Khayat, A. Derdouri, B. Peseux, Dynamic inflation of hyperelastic spherical membranes, J. Rheol. 43 (1999) 1083–1097.

[29] E. Verron, G. Marckmann, B. Peseux, Dynamic inflation of non-linear elastic and viscoelastic rubberlike membranes, to be published in Int. J. Numer. Meth. Engng.

[30] A. Wineman, On axisymmetric deformations of nonlinear viscoelastic membranes, J. Non-Newtonian Fluid Mech. 4 (1978) 249–260.

[31] P. Wriggers, R. L. Taylor, A fully nonlinear axisymmetrical membrane element for rubber-like material, Engng Comput. 7 (1990) 303–310.

[32] W. H. Yang, W. W. Feng, On axisymmetrical deformations of nonlinear membranes, J. Appl. Mech. ASME 37 (1970) 1002–1011.